Hindawi Publishing Corporation
Advances in Materials Science and Engineering
Volume 2016, Article ID 3701292, 17 pages
http://dx.doi.org/10.1155/2016/3701292

Research Article

Pilot Study for Investigating the Cyclic Response of the Recentering Bridge Bearing System Combined with the Friction Damper

Jong Wan Hu[1,2] and Yong-il Cho[1]

[1]*Department of Civil and Environmental Engineering, Incheon National University, Incheon 22012, Republic of Korea*
[2]*Incheon Disaster Prevention Research Center, Incheon National University, Incheon 22012, Republic of Korea*

Correspondence should be addressed to Jong Wan Hu; jongp24@incheon.ac.kr

Received 11 May 2016; Revised 24 July 2016; Accepted 8 August 2016

Academic Editor: Pavel Lejcek

The bridge bearing is one of the component members which provide resting supports between piers and decks. The bridge bearing is intended to control longitudinal movement caused by traffic flow and thermal expansion, thereby reducing stress concentration. In high seismicity area, the bridge bearing has been utilized as the base isolation system to mitigate acceleration transferred from the ground. Although the existing bridge bearing installed between superstructure and substructure provides extra flexibility to the base of the entire structure, considerable permanent deformation occurs due to lack of recentering capacity after earthquake. It is required to spend extra cost for repairing impaired parts. The bridge bearings integrated with superelastic shape memory alloy (SMA) devices used for upgrading the recentering effect into the friction damper are proposed in this study. The refined finite element (FE) analyses are introduced to reproduce the response of such new structures under cyclic loading condition. The bridge bearing systems that maintain uniform recentering capability are designed with various friction coefficients so as to examine energy dissipation and residual deformation through FE analyses. After observing FE analysis results, optimal design for the recentering bridge bearing system will be proposed to take advantage of energy dissipation and self-centering capacity.

1. Introduction

Typical bridge bearings which are placed in between girders and piers uphold the gravity load and permit additional flexibility to damp dynamic impact caused by vehicle movements [1–3]. In addition, these bridge bearings can properly deal with the deformation of the superstructure (i.e., girder, pavement, and deck), which mostly arises from creep, shrinkage, and temperature change [4, 5]. Therefore, they have been recognized as one of the mechanical devices to minimize the occurrence of supplemental stress in the bridge. As the length of the bridge span has been recently increasing in the construction field, the gravity load upheld by the bridge bearing increases as well. Accordingly, several types of the bridge bearings have been developed so as to accommodate complex mechanism and load distribution caused by supporting these structures. The bridge bearing installed under the steel box girder is shown in Figure 1.

The seismic load imposed on the structure is the most dominant over other types of the loads, and it is thus important to act as the passive control system that isolates the transferred acceleration from the ground [6–8]. In high seismicity area, the bridge bearing has been utilized as the base isolation device designed to alleviate the damage of the entire structure by reducing the ground acceleration transferred to the superstructure of the bridge [9]. The base bearing systems which are made up of flexible components allow the movement along the direction of the earthquake, thereby increasing the fundamental period of the base-isolated structure. In general, response acceleration spectra have a tendency to be weakened at the relatively long fundamental period [8, 10, 11]. Accordingly, bridge bearings

Figure 1: Bridge bearing installed under the steel box girder.

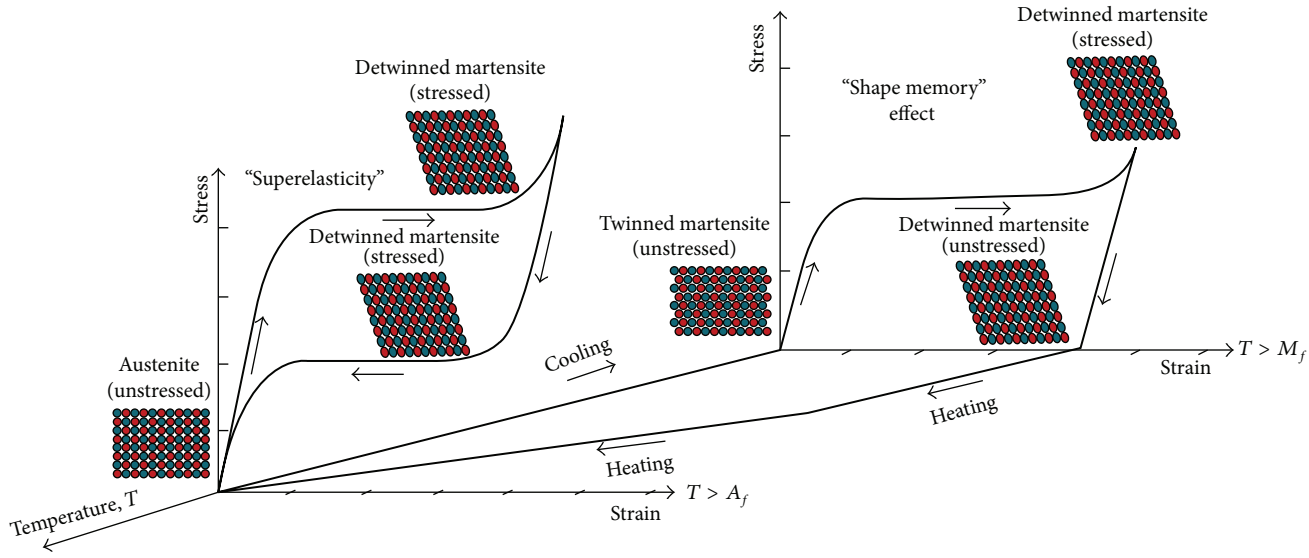

Figure 2: Stress and strain curves for shape memory alloy (SMA) materials.

make a significant contribution to mitigating seismic force converted from ground acceleration. Besides, these bridge bearings function as the dampers that can dissipate a considerable amount of energy for the purpose of absorbing the impact quickly. In spite of the established bearing systems having flexibility and energy dissipation capacity, they display the significant drawback of generating residual deformation resulting from the lack of the recentering capability, and thus the extra cost may be required to restore the original configuration [11–13]. For this reason, new bridge bearing systems integrated with superelastic SMA devices are proposed in this study.

The SMAs as one of the smart materials can go back to original condition with nearly zero residual strain after heating or the removal of stress. The stress and strain curves for typical SMA materials are presented in Figure 2. When SMA materials are applied to displacement loads exceeding the elastic range, residual deformation occurs below the martensite phase transformation temperature ($T > M_f$) after removing the applied loads [14, 15]. The shape memory effect is displayed at the SMAs with martensite phase transformation, indicating that additional heat treatment shall be given in an effort to return to their original configuration. Above the austenite phase transformation ($T > A_f$), superelastic effect that can automatically recover to original configuration without heat treatment is shown at the SMA [15]. The superelastic SMAs currently developed are able to maintain austenite phase transformation at room temperature, accommodate up to 8% plastic strain by undergoing a stress plateau, and finally behave like the flag-shaped hysteresis loop with nearly zero residual strain upon unloading. These unique material characteristics will be taken into consideration for bearing design.

The new bridge bearing systems that are integrated with recentering capability attributed by superelastic SMA bars and energy dissipation capacity attributed by friction dampers are proposed in this study. Instead of experimental tests, the behavior of such new systems is simulated by refined 3-dimensional (3D) finite element (FE) analyses. The friction damper which is one of the representative displacement control devices based on energy dissipation contributes to alleviating vibration by absorbing external impact but is concerned with generating residual deformation. The bearing models are designed with variable friction coefficients in

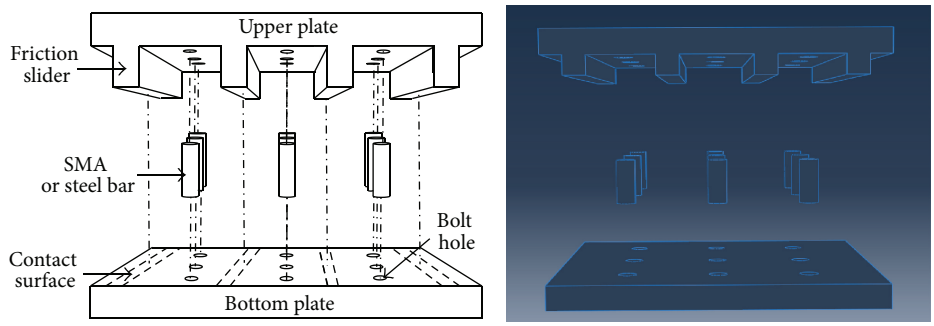

Figure 3: 3D schematic drawing for bearing components.

an effort to investigate whether recentering capability has a direct relationship to energy dissipation capacity obtained from friction mechanism in the new bridge bearing. In addition, the comparative bearing models utilizing conventional steel bars are also set to validate the recentering effect guaranteed by superelastic SMA bars. After simulating the behavior of individual bridge bearing models through 3D refined nonlinear FE analyses, mechanical performances with respect to energy dissipation, ultimate strength, residual displacement, and recentering capability are compared to each other. The axial stress-strain field contours distributed over the bridge bearing models as well as the stress-strain hysteresis curves measured at the specific points are also investigated to verify the adequacy of FE models. Finally, the optimal design method for the recentering bridge bearing systems will be proposed in order to make the best use of both energy dissipation and recentering effect.

2. Bearing Design

The new bridge bearing systems which are equipped with recentering devices made by superelastic SMA and friction dampers used for energy dissipation are proposed in this study. 3D schematic drawing for bearing components is illustrated in Figure 3. Rectangular sliders engendering frictional response are connected to the upper plate by welding. The circular bars fabricated with conventional steel or superelastic SMA are installed in between upper plate and bottom plate with the aim of controlling lateral displacement. Including the friction sliders, the circular bars directly support gravity loads along the vertical direction. The friction forces occurring along the horizontal (or shear) direction are regulated by changes in the friction coefficient, which is determined by the condition of the contact surface between the friction slider and the bottom plate. The change in the friction force can be achieved by embrocating lubricants on the contact surfaces. It is another method to change friction force that thin grooves on the contact surfaces are constructed so as to reduce the gravity load supported by the friction slide. Once SMA bars are connected to both plates by welding, their material properties will be changed by heat treatment [14, 15]. The bolt holes are perforated to both plates as shown in the figure, and then the circular bars are inserted into these bolt holes for the purpose of connecting them to the plates without heat treatment. The bearing systems with conventional steel bars are additionally designed to compare those with superelastic SMA bars in terms of recentering capability and energy dissipation capacity. These circular bars supply additional strength to resist shear force and effectively absorb dynamic impact during metallic yielding.

The sizes of component members composing the bearing model presented herein are illustrated in Figure 4. The practical use in the construction field is taken into consideration for manufacture, and thus the bearing systems are designed with relatively simple component members. These bearing systems are basically designed to support 981 kN gravity load, sustaining the elastic state. Nine circular bars with 25.4 mm diameter are inserted into boles perforated with 25.4 mm diameter and 25 mm depth. The spacing and alignment of the circular bars are described in the plan view with further details. The upper and bottom plates are fabricated with the size of 450 mm width, 500 mm length, and 50 mm thickness. Four friction sliders are designed with 30 mm width, 500 mm length, and 40 mm height and directly connected to the upper plate by welding. The upper and bottom plates are fabricated with general carbon steel (i.e., Gr. 50 steel) or corrosion-free stainless steel. Based on the design of such bridge bearing systems, their response mechanism will be described in the following section.

3. Response Mechanism

The total behavior of the bridge bearing has an influence on the behavior of individual components (i.e., circular bars and friction sliders) and is reproduced by assembling components' behaviors in parallel. Including the assemblage of the component members, the response mechanism of the bridge bearing is presented in Figure 5. The steel and superelastic SMA bars subjected to shear and bending have response mechanism based on their own material behavior. Accordingly, the behavior of the steel bars can be defined as the hysteresis loop including isotropic hardening and Bauschinger effect. On the other hand, that of the superelastic SMA bars can be characterized by the flag-shaped hysteresis loop with the stress plateau. The friction sliders abruptly start to move when shear force applied to the bridge bearing exceeds slip resistance. For this reason, the behavior of the friction sliders can be simply idealized by the rectangular

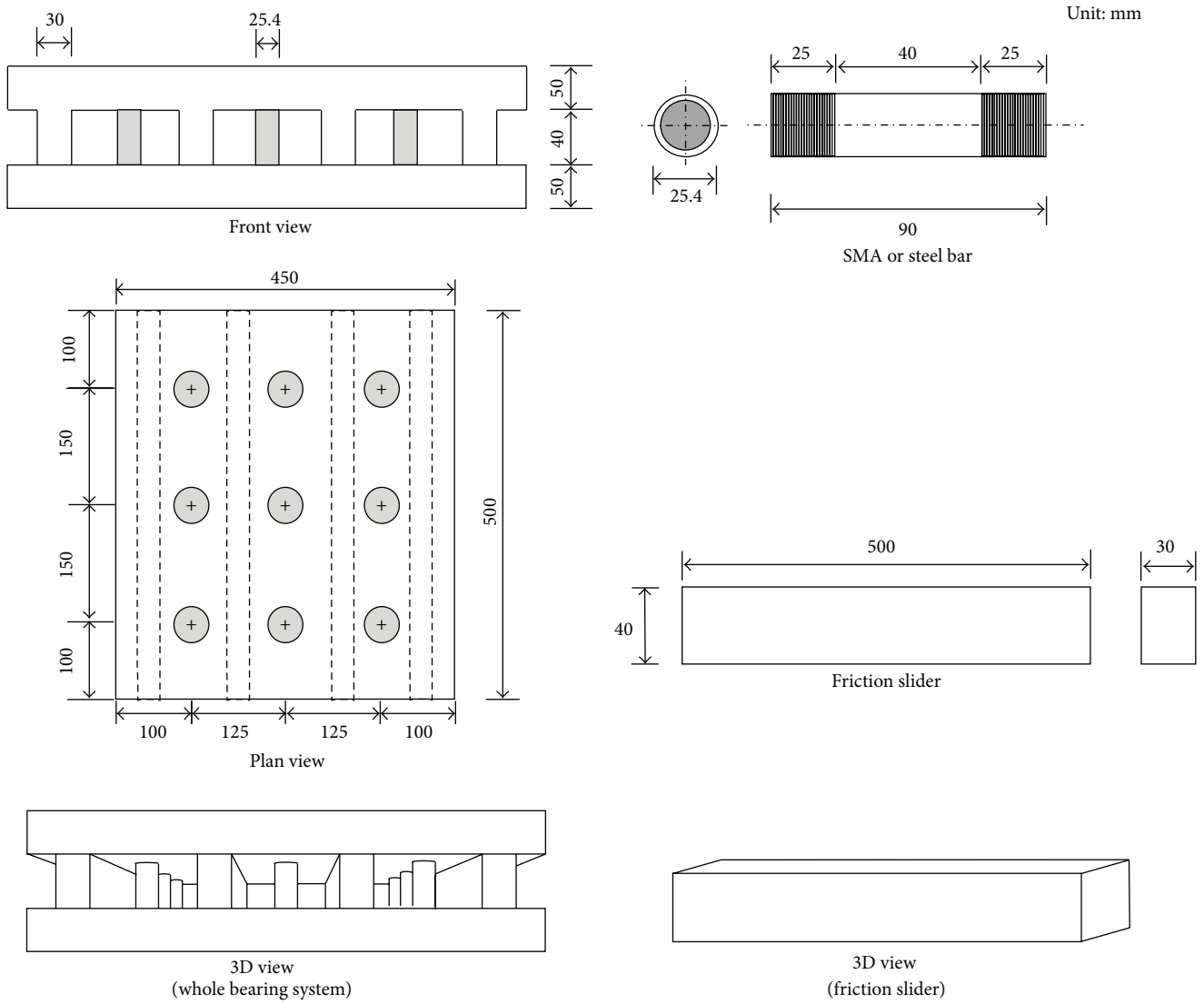

Figure 4: Design of the recentering bridge bearing combined with the friction slider system.

hysteresis loop defined as slip distance and slip resistance. The amount of energy dissipation, which is represented by the area of the rectangular hysteresis loop, is simply regulated by the depth of the groove on the contact surface.

As presented in (1) associated with Figure 5, the total behavior of the bridge bearing can be also reproduced by superposing two component forces in parallel at the fixed displacement. In spite of increasing energy dissipation capacity and internal resistance against external force, it is expected that steel bars installed in the bridge bearing give rise to permanent deformation due to metallic yielding. However, bridge bearings equipped with the superelastic SMA bars lead to reducing the outbreak of permanent deformation owing to recentering force. In addition, their flag-shaped hysteresis behavior can provide supplemental damping attributed by dissipating energy to the bearing system. The postyield strength of the superelastic SMA is relatively larger than that of typical carbon steel, and thus the proposed recentering bridge bearing possesses enough internal strength to resist external force more effectively:

$$\begin{aligned} F &= F_{\mathrm{STE}} + F_{\mathrm{fric}}, \\ F &= F_{\mathrm{SMA}} + F_{\mathrm{fric}}, \\ \Delta &= \Delta_{\mathrm{STE}} = \Delta_{\mathrm{SMA}} = \Delta_{\mathrm{fric}}. \end{aligned} \tag{1}$$

In this study, bridge bearing models designed with the same friction conditions but with the difference bar materials are compared and evaluated in terms of performance and response through FE analyses. The model identifications (IDs) are also presented in Figure 5. The first acronym shown in the model ID represents the type of the circular bar devices installed in the bridge bearing. The STE series models indicate the bridge bearings equipped with the steel bars while these with the superelastic SMA bars are classified as the SMA series models. The second acronym represents

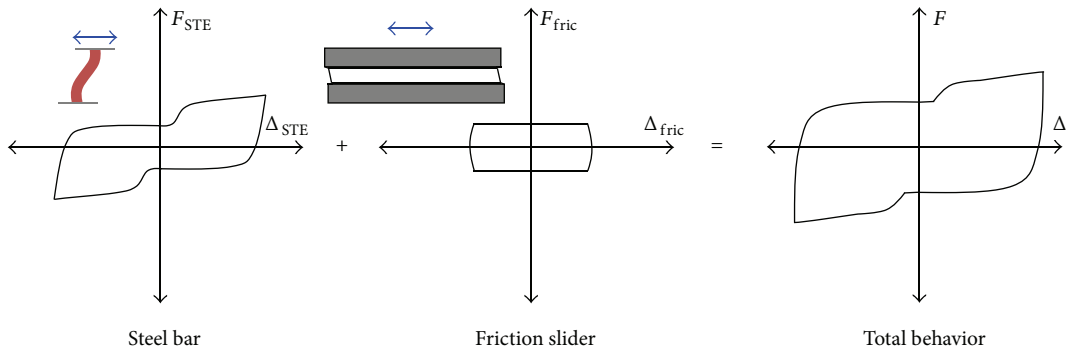

(a) Steel bearing model with friction slider (STE-0.00, STE-0.05, STE-0.10, . . ., and STE-0.40 models)

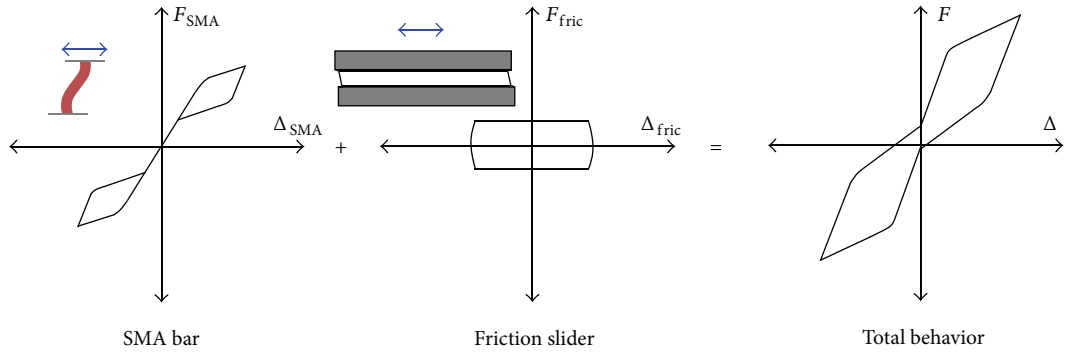

(b) SMA bearing model with friction slider (SMA-0.00, SMA-0.05, SMA-0.10, . . ., and SMA-0.40 models)

Figure 5: Response mechanism of the bridge bearing.

the values of the friction coefficients applied to the contact surface between friction slider and bottom plate. Nine bridge bearing models with steel or superelastic SMA bars are constructed with variable friction coefficients ranging from 0 to 0.4, as increasing by 0.05, respectively. It is intended to examine the change of the total response in the bridge bearing according to the variable friction condition when resistance strength provided by the circular bars keeps a constant level.

4. Finite Element Models

As a pilot research, bridge bearing systems with recentering capability are newly suggested in this study, and then their responses under cyclic loading are predicted through refined 3D FE analyses. This preliminary research stage is necessary to verify the adequacy of structural design for smart systems based on their response mechanism with respect to recentering and energy dissipation prior to experimental tests performed to predict their real behavior physically. In lieu of the experimental tests, this study conducts nonlinear FE analyses with the aim of simulating the behavior of the proposed bridge bearing system. Eighteen FE models composed of nine bridge bearings equipped with conventional steel bars and nine bridge bearings with superelastic SMA bars were constructed for these numerical analyses. In a way of FE modeling, it is important to save time and cost with accurate prediction. The superstructures (e.g., steel girder, deck, and pavement) supported by the bridge bearings can be replaced with the gravity load, because the FE analyses performed in this study just focus on its own response of the bridge bearing system. In addition, the substructures (e.g., pier and abutment) are replaced with boundary conditions (BCs), thus omitting achieving detail modeling. The Abaqus program was used to perform the FE analyses [16].

The refined 3D FE models for the bridge bearings are shown in Figure 6. Element meshes, loading, and BCs are also shown in this figure. The FE models are made up of 8-node solid elements with nonlinear material properties. These solid elements were generated by using structural mesh division in an effort to converge analysis results quickly. The first static time step was defined to take the gravity loads transferred from the supported superstructures into consideration for FE analyses. The uniform pressure for simulating the gravity load was applied to the top surface of the upper plate. After completing the first static time step for applying the gravity loads, the second static time step was applied to impose displacement-controlled cyclic loads with the time history on the upper plate along the horizontal (or shear) direction. The reaction force loads were measured using the history output provided in the Abaqus program. The fixed BCs imposed on the bottom plate were modeled to replace the substructure to save time and cost. The contact surfaces where two independent parts touched together were modeled using the surface interaction, and geometric nonlinearity was taken into consideration for accurate FE analyses.

In addition to geometric nonlinearity, material nonlinearity was also taken into account during FE modeling for the purpose of conducting accurate prediction. Including steel

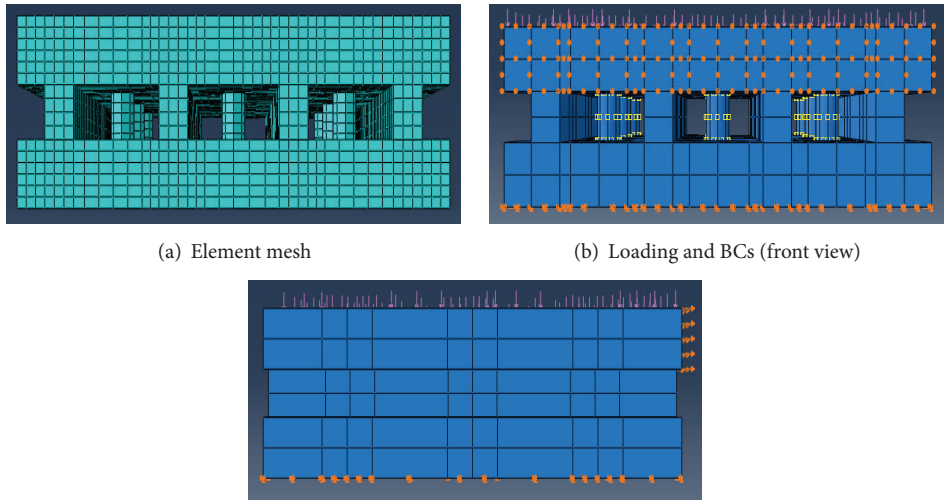

(a) Element mesh

(b) Loading and BCs (front view)

(c) Loading and BCs (side view)

Figure 6: Finite element models.

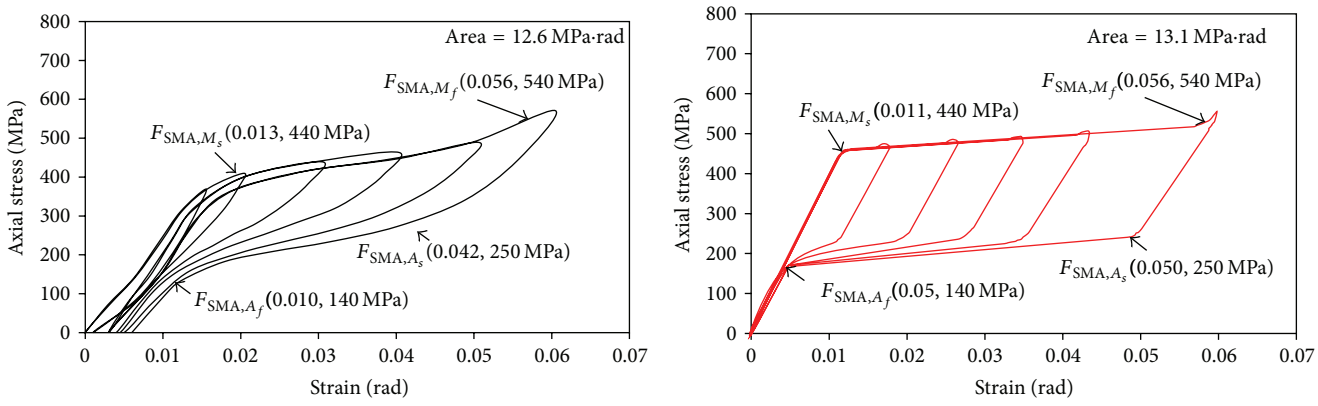

(a) Experimental curve

(b) Simulated curve

Figure 7: Simulated superelastic SMA curves.

bars and friction sliders, both steel plates were fabricated with Gr. 50 carbon steel which possesses 345 MPa yield stress, 200 GPa elastic modulus, and 1.5% strain hardening ratio. The behavior of this steel material was simulated using the isotropic hardening model, which exhibits stress relaxation, Bauschinger effect, and ratcheting response provided by the Abaqus program. The nonlinear material properties were aligned to individual parts (i.e., plates, sliders, and steel bars) composed of 3D solid elements. The default material model used to reproduce the behavior of the superelastic SMA material is absent in the program, and thus the user-defined material (UMAT) model reflecting phase transformation was employed to FE modeling [17, 18]. The material input properties required to operate the UMAT model were obtained from uniaxial pull-out tests performed by DesRoches et al. [15]. The stress and strain curves for superelastic SMA materials are presented in Figure 7. The material input properties required to simulate the behavior of the superelastic SMA during FE analyses were taken as the values of 40 GPa for elastic modulus, 0.33 for Poisson's ratio, 440 MPa for martensite start stress, 540 MPa for martensite finish stress, 250 MPa for austenite start stress, 140 MPa for austenite finish stress, 0.045 radians for transformation strain, and 25°C for transformation reference temperature. The simulated stress and strain curve was represented by a series of straight lines, which coincide with the path of each phase transformation. Overall, the simulated curve shows a good agreement with the experimental curve.

The hysteresis loops that are able to evaluate energy dissipation capacity and recentering capability for individual bridge bearing models are simulated to impose the pseudo-static cyclic loads with the displacement loading history on the upper plate. In order to verify reliable FE modeling, it is important to check whether the stress and strain curves measured from the specific point are in conformity with the behavior of the base material. The displacement loading

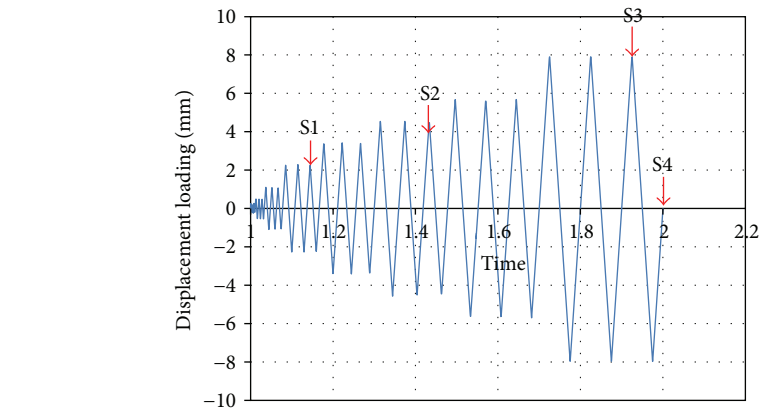

(a) Displacement loading history

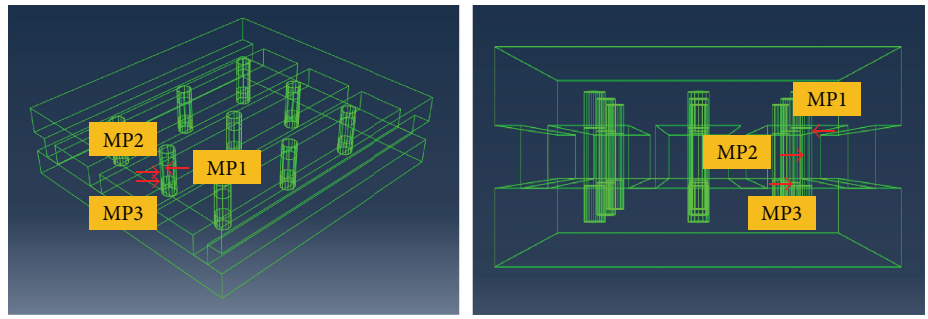

(b) Measurement points

Figure 8: Displacement loading history and measurement points for data collection.

history and measurement points for data collection (i.e., MP1, MP2, and MP3) are shown in Figure 8. As the number of loading cycles increases, the amplitude of the load gradually increases to 8 mm displacement. The displacement loading history was generated by using the amplitude function in the program and associated with the displacement-controlled cyclic loads as shown in Figure 8. The axial strain and stress field contours distributed over the bridge bearing were examined at the specific displacement loads (i.e., S1, S2, S3, and S4 shown in Figure 8(a)). Finally, the measurement points used to collect the data of axial stress and strain were set up at middle and end points of the circular bars considering their deformation caused by shear and bending (see Figure 8(b)).

5. Analysis Results

The FE analyses were conducted by applying the displacement-controlled cyclic loads to the upper plate, and then the obtained analysis results are investigated in this section. The FE models behave as the closed-symmetric hysteresis loops under tension and compression, thereby confirming their energy dissipation capacity and recentering capability at these hysteresis loops. The behavior of steel and superelastic SMA bars, which was simulated by FE models without friction mechanism (e.g., STE-0.00 and SMA-0.00 models), is presented in Figure 9. The deformable contributions are caused by shear and bending. The behavior of such bridge bearing models is only affected by the material property of the circular bars due to absence of the friction mechanism. The STE-0.00 model with the steel bars shows strain hardening and Bauschinger effect at the hysteresis loop while the SMA-0.00 model with the superelastic SMA bars exhibits the flag-shaped hysteresis loop corresponding to material behavior. In spite of creating more energy dissipation, the former STE-0.00 model generates a considerable amount of residual displacement. Contrarily, the latter SMA-0.00 model is able to recover to its original condition with nearly zero residual displacement upon unloading. This model produces about 120 kN recentering force during reverse phase transformation from martensite to austenite. The recentering force can help offset residual displacement caused by friction mechanism in the bearing system and thus makes a significant contribution to recovering the structural damage.

It is also necessary to investigate the effect of friction mechanism, which is represented by additional energy dissipation in the total hysteresis loop. As increasing friction forces is the variable parameter in the bridge bearing, definite changes in the hysteresis loops are investigated with constant strength capacity provided by the circular bars. The hysteresis loops simulated by the FE analyses are presented in Figures 10 and 11. Figure 10 shows the total behavior of the bearing systems equipped with the steel bars while Figure 11 shows the total behavior of the bearing systems equipped with the superelastic SMA bars. On the basis of the hysteresis loop presented in Figure 9(a), ultimate strength measured at 8 mm

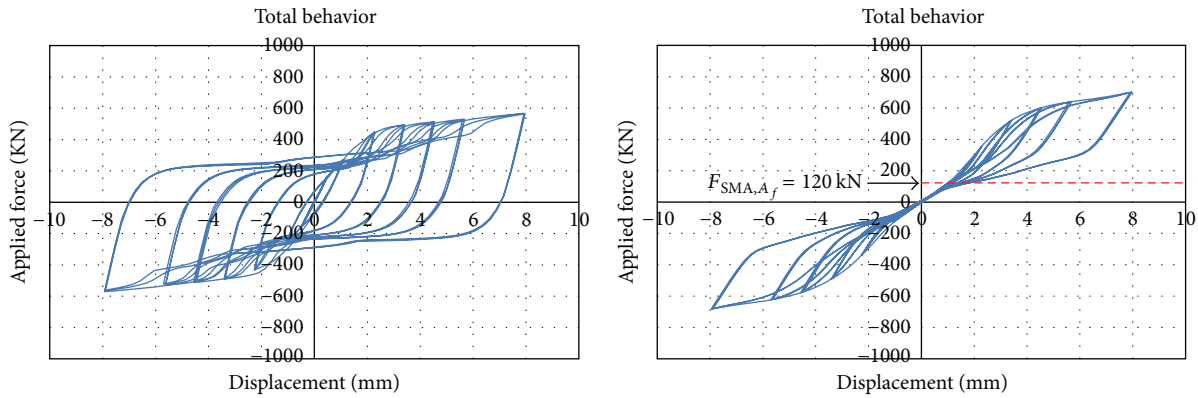

(a) STE-0.00 model (b) SMA-0.00 model

Figure 9: Total behavior of the bearing systems without friction mechanism.

displacement ascends as the friction coefficient of the FE model shifts from low level to high level. For instance, the STE-0.00 model with zero-friction mechanism has 565 kN force at 8 mm displacement while the STE-0.40 model has as much as 972 kN force. Therefore, friction mechanism occurring at the contact surface between the friction slider and the bottom plate makes a big contribution to augmenting postyield strength sharply. All of the STE series models behave as the symmetric hysteresis loops with definite strain hardening and Bauschinger effect. However, these STE series models are not recovered to their original configuration and still have considerable amount of residual displacement upon unloading. The inherent behavior characteristic of these STE series models is that the initial slopes are almost the same as the unloading slopes. Thus, residual displacement ascends more and more as applied displacement increases before unloading.

The hysteresis loops for the bridge bearing models with the superelastic SMA bars are also investigated as varying friction coefficients. As can be seen in Figure 11, increasing the friction coefficient leads to ascending ultimate strength measured at 8 mm displacement as well. The SMA-0.00 with zero-friction mechanism has 702 kN force while the SMA-0.40 model has as much as 1078 kN force. The friction mechanism applied to the recentering bearing system contributes to upgrading resistance against external force as well as to expanding the area of the hysteresis loop, meaning that energy dissipation capacity can be improved. However, increasing friction force leads to the degradation of recentering capacity and thus causes augmenting residual displacement upon unloading. The friction coefficient exceeding 0.2 starts to rapidly increase residual displacement at the hysteresis loop and considerably lose the recentering capability. As the number of loading cycles increases, residual displacement generally increases as well. Although the superelastic SMA bars provide recentering effect on the bearing system, once friction force that resists slip movement exceeds recentering force, residual displacement takes place under cyclic loads. Comparing FE bearing models with the steel bars under the same friction coefficient, in general, those with the superelastic SMA bars show relatively smaller residual displacement at the hysteresis loop. For example, the STE-0.40 model generates 7.7 mm residual displacement upon unloading from 8 mm maximum displacement while the SMA-0.40 model has about 6.5 mm residual displacement under the same unloading path.

The response mechanisms for individual components (i.e., bars and friction sliders) have an influence on formulating the behavior of the bridge bearing system, and thus it is necessary to investigate relationship between total behavior and component behavior. It is also necessary to check whether or not an assemblage of individual components in parallel coincides with the behavior of the bridge bearing. The simulated curves for the behavior of individual components and the total behavior of the specific model cases are presented in Figures 12 and 13. Residual displacements (Δ_{res}), maximum forces (F_{max}), and maximum displacements (Δ_{max}) are denoted in the figures, and their specific values are summarized according to individual models in Tables 1 and 2. As defined in (2) indicating parallel assembly relation, the resultant forces of the steel (or superelastic SMA) bars and the friction sliders are almost equal to the forces of the bearing models under the same displacement points. In addition to Figures 12 and 13, this statement can be identified in Tables 1 and 2 as well. In general, the SMA series models display larger postyield strength than the STE series models under the same friction condition because the superelastic SMA bars provide more strength capacity than the steel bars in the bearing system. Friction forces (F_{fric}) are nearly identical to forces computed by the product of the friction coefficient and the gravity load. As we expected, bridge bearing models with the superelastic SMA bars show better recentering capability than those with the steel bars because they generate recentering forces against friction resistance during cyclic loading tests

$$F_{max} = F_{STE,max} + \left|F_{fric,max}\right|,$$
$$F_{max} = F_{SMA,max} + \left|F_{fric,max}\right|. \quad (2)$$

The recentering ratios (RRs; see (3)) and energy ratios (ERs; see (4)) are also summarized in Tables 1 and 2. As

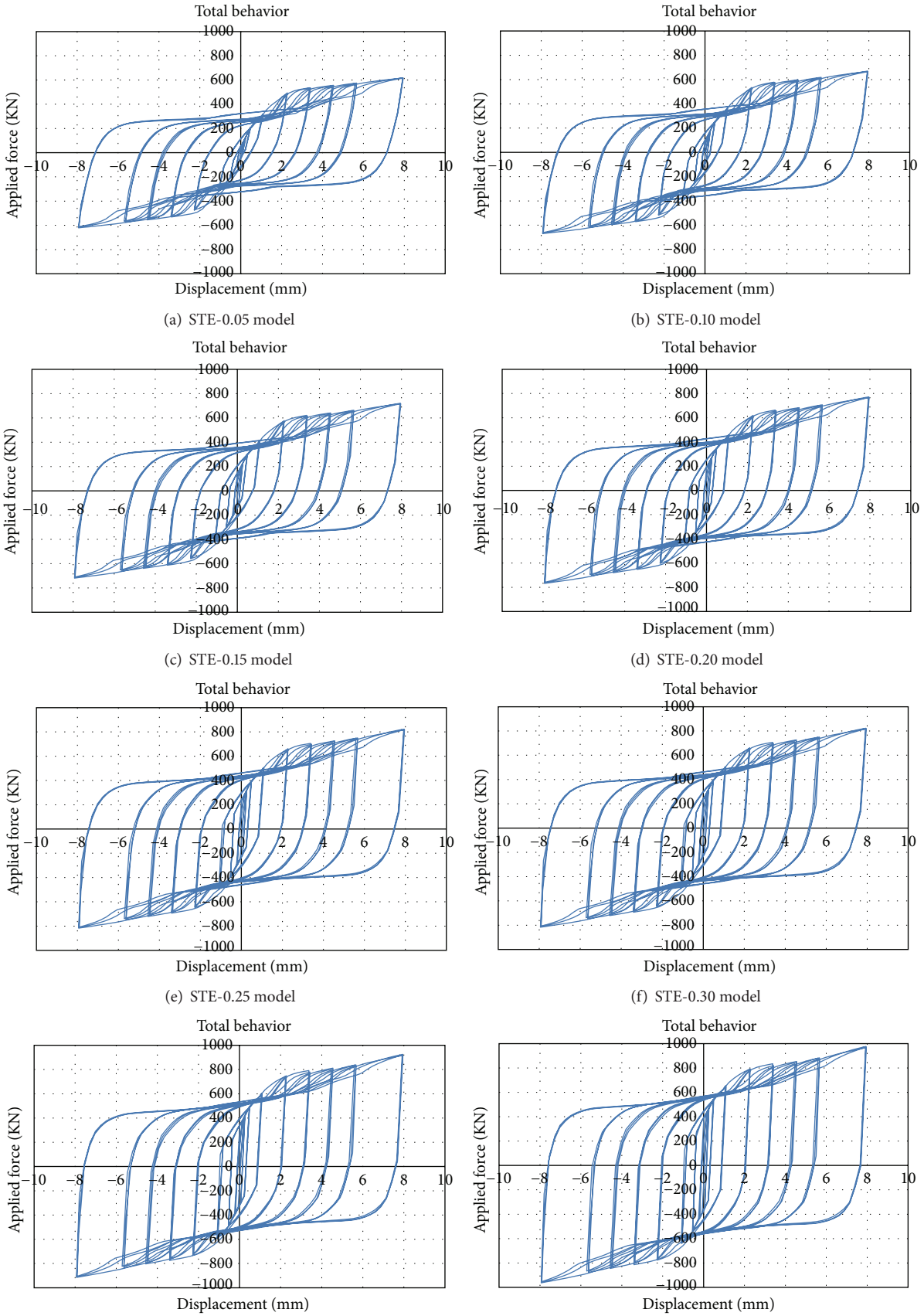

(a) STE-0.05 model

(b) STE-0.10 model

(c) STE-0.15 model

(d) STE-0.20 model

(e) STE-0.25 model

(f) STE-0.30 model

(g) STE-0.35 model

(h) STE-0.40 model

Figure 10: Total behavior of the traditional steel bearing systems with the friction damper.

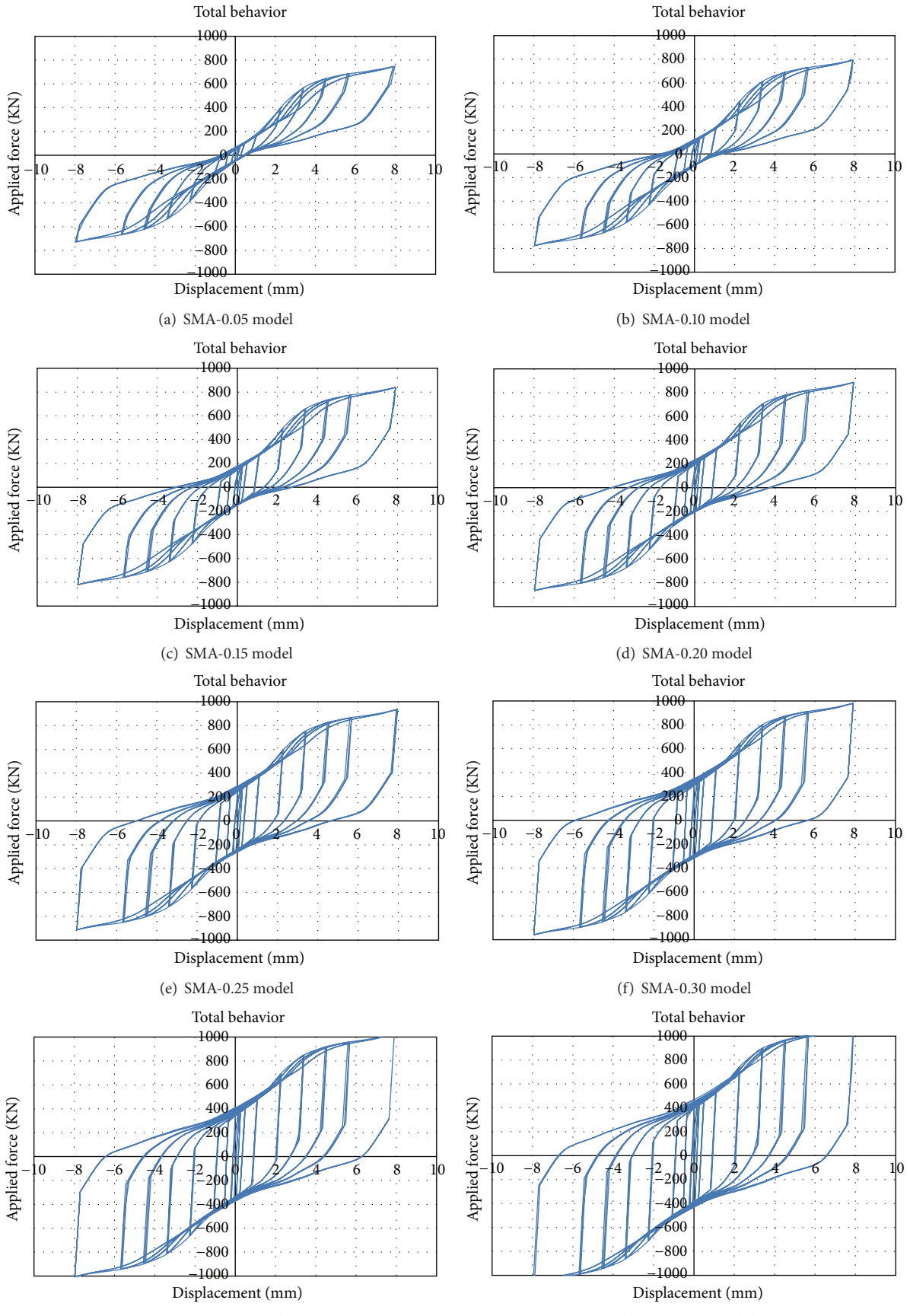

(a) SMA-0.05 model

(b) SMA-0.10 model

(c) SMA-0.15 model

(d) SMA-0.20 model

(e) SMA-0.25 model

(f) SMA-0.30 model

(g) SMA-0.35 model

(h) SMA-0.40 model

Figure 11: Total behavior of the superelastic SMA bearing systems with the friction damper.

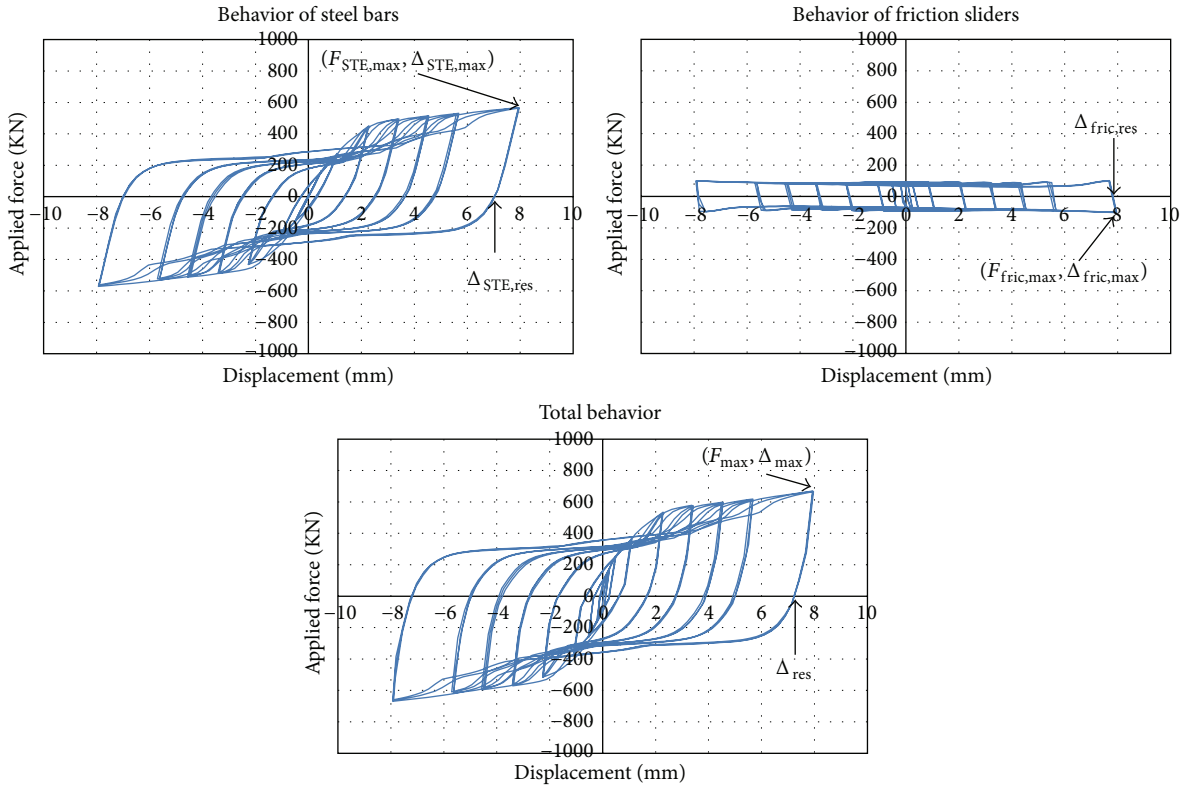

(a) STE-0.10 model

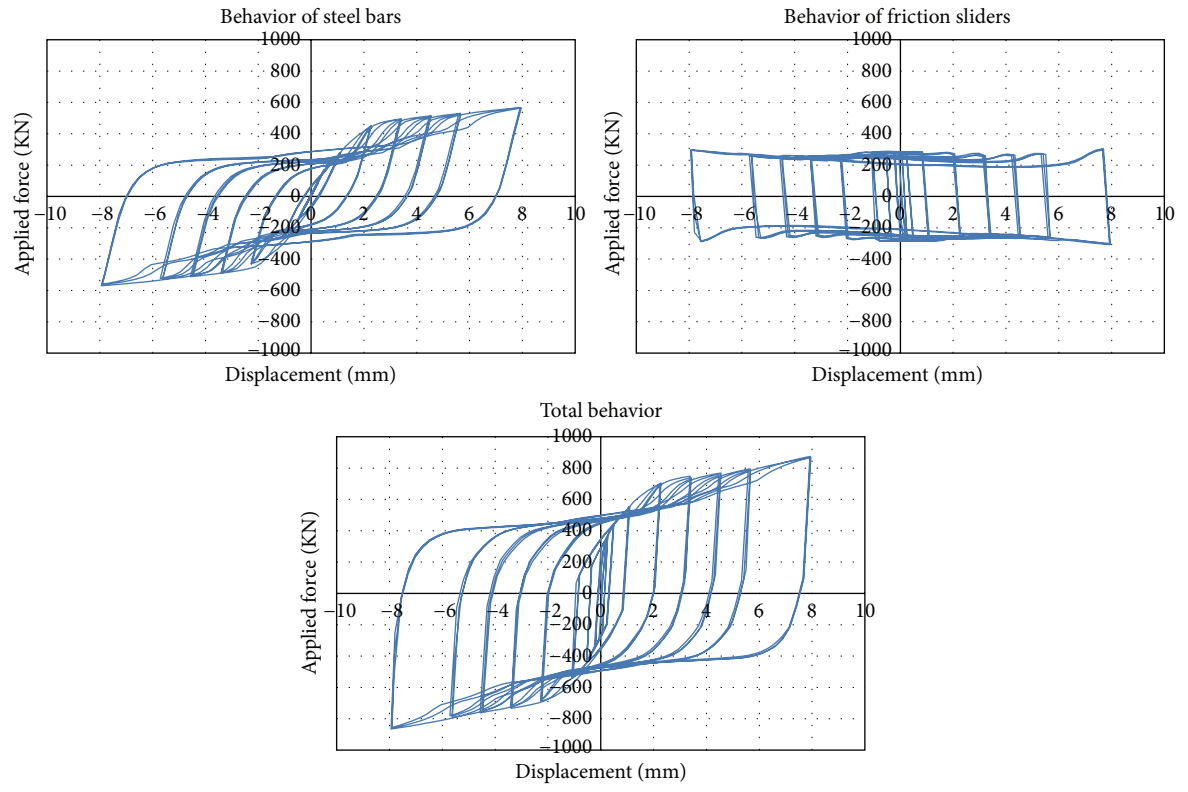

(b) STE-0.30 model

FIGURE 12: Simulated curves for the behavior of individual components and the total behavior of the specific model cases (STE-0.10 and STE-0.30 models).

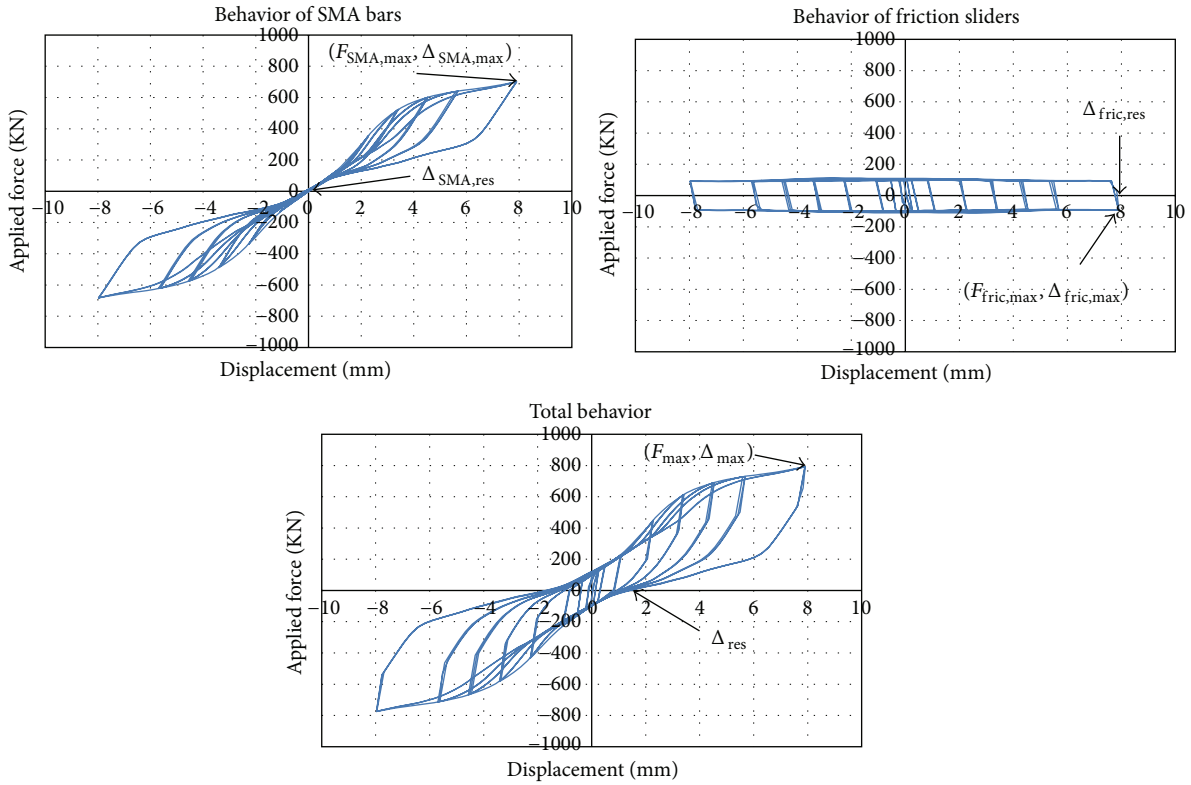

(a) SMA-0.10 model

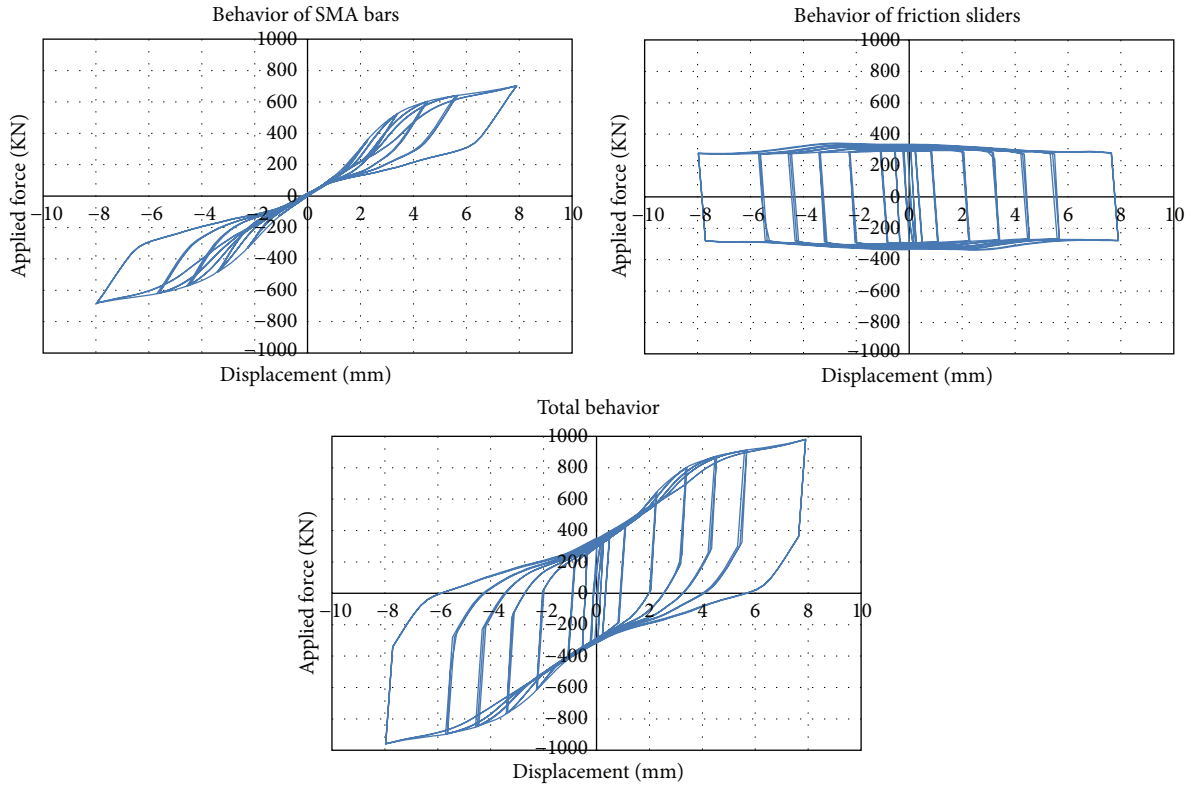

(b) SMA-0.30 model

Figure 13: Simulated curves for the behavior of individual components and the total behavior of the specific model cases (SMA-0.10 and SMA-0.30 models).

Table 1: Summarized analysis results for the steel bearing systems.

Model ID	Behavior of steel bars			Behavior of friction sliders			Total behavior					
	$F_{STE,max}$	$\Delta_{STE,max}$	$\Delta_{STE,res}$	$F_{fric,max}$	$\Delta_{fric,max}$	$\Delta_{fric,res}$	F_{max}	Δ_{max}	Δ_{res}	RR	Energy (area)	ER
STE-0.00	564.6 kN	8.0 mm	6.9 mm	0.0 kN	0.0 mm	0.0 mm	564.6 kN	8.0 mm	6.9 mm	13.3%	10250.0 kN-mm	0.0%
STE-0.05	564.6 kN	8.0 mm	6.9 mm	−50.8 kN	8.0 mm	7.7 mm	615.4 kN	8.0 mm	7.2 mm	10.0%	11300.0 kN-mm	10.2%
STE-0.10	564.5 kN	8.0 mm	6.9 mm	−101.7 kN	8.0 mm	7.7 mm	666.2 kN	8.0 mm	7.2 mm	10.0%	12475.0 kN-mm	21.7%
STE-0.15	564.4 kN	8.0 mm	6.9 mm	−152.7 kN	8.0 mm	7.7 mm	717.1 kN	8.0 mm	7.4 mm	6.6%	13750.0 kN-mm	34.1%
STE-0.20	564.3 kN	8.0 mm	6.9 mm	−203.7 kN	8.0 mm	7.7 mm	768.0 kN	8.0 mm	7.4 mm	6.6%	14975.0 kN-mm	46.1%
STE-0.25	564.1 kN	8.0 mm	6.9 mm	−254.6 kN	8.0 mm	7.7 mm	818.8 kN	8.0 mm	7.4 mm	6.6%	16050.0 kN-mm	56.6%
STE-0.30	564.0 kN	8.0 mm	6.9 mm	−305.7 kN	8.0 mm	7.7 mm	869.8 kN	8.0 mm	7.4 mm	6.6%	17425.0 kN-mm	70.0%
STE-0.35	563.9 kN	8.0 mm	6.9 mm	−356.9 kN	8.0 mm	7.7 mm	920.8 kN	8.0 mm	7.7 mm	3.3%	18575.0 kN-mm	81.2%
STE-0.40	563.8 kN	8.0 mm	6.9 mm	−408.2 kN	8.0 mm	7.7 mm	972.0 kN	8.0 mm	7.7 mm	3.3%	19650.0 kN-mm	91.7%

Table 2: Summarized analysis results for the SMA bearing systems.

Model ID	Behavior of SMA bars			Behavior of friction sliders			Total behavior					
	$F_{SMA,max}$	$\Delta_{SMA,max}$	$\Delta_{SMA,res}$	$F_{fric,max}$	$\Delta_{fric,max}$	$\Delta_{fric,res}$	F_{max}	Δ_{max}	Δ_{res}	RR	Energy (area)	ER
SMA-0.00	701.9 kN	8.0 mm	0.0 mm	0.0 kN	0.0 mm	0.0 mm	701.9 kN	8.0 mm	0.0 mm	100.0%	3575.0 kN-mm	0.0%
SMA-0.05	702.4 kN	8.0 mm	0.0 mm	−45.9 kN	8.0 mm	7.8 mm	748.3 kN	8.0 mm	0.6 mm	93.1%	5050.0 kN-mm	41.3%
SMA-0.10	700.4 kN	8.0 mm	0.0 mm	−91.9 kN	8.0 mm	7.8 mm	792.2 kN	8.0 mm	1.2 mm	84.7%	6725.0 kN-mm	88.1%
SMA-0.15	700.7 kN	8.0 mm	0.0 mm	−138.0 kN	8.0 mm	7.6 mm	838.7 kN	8.0 mm	2.8 mm	64.5%	8100.0 kN-mm	126.6%
SMA-0.20	701.2 kN	8.0 mm	0.0 mm	−185.3 kN	8.0 mm	7.6 mm	886.5 kN	8.0 mm	3.7 mm	53.5%	9550.0 kN-mm	167.1%
SMA-0.25	703.7 kN	8.0 mm	0.0 mm	−232.4 kN	8.0 mm	7.7 mm	936.1 kN	8.0 mm	4.6 mm	42.3%	11225.0 kN-mm	214.0%
SMA-0.30	702.2 kN	8.0 mm	0.0 mm	−279.2 kN	8.0 mm	7.6 mm	981.4 kN	8.0 mm	5.8 mm	26.8%	12800.0 kN-mm	258.0%
SMA-0.35	702.8 kN	8.0 mm	0.0 mm	−326.5 kN	8.0 mm	7.6 mm	1029.3 kN	8.0 mm	6.3 mm	20.1%	14325.0 kN-mm	300.7%
SMA-0.40	703.5 kN	8.0 mm	0.0 mm	−374.0 kN	8.0 mm	7.8 mm	1077.5 kN	8.0 mm	6.5 mm	17.7%	15800.0 kN-mm	342.0%

presented in (3), the recentering ratios are defined as the maximum recoverable displacement divided by the maximum displacement. The energy ratios defined in (4) are presented to examine the portion of friction mechanism, which is occupied at the behavior of the bearing model. The amount of energy dissipation presented in these tables (E) is determined by the area of the hysteresis loop in the bridge bearing model. The STE series models dissipate relatively more kinetic energy than the SMA series models under the same friction condition owing to excellent metallic yielding obtained from the steel bars. This will result in reducing reliance on energy dissipation from friction mechanism as presented in the energy ratio. Although the STE series models possess superior energy dissipation capacity to absorb impact and vibration to the SMA series models, they have some drawbacks related to the occurrence of more residual displacement. The steel bars have smaller postyield strength to resist shear and bending compared to the superelastic SMA bars under the same displacement. Accordingly, the STE series models are more susceptible to strong seismic force and more vulnerable to severe structural damage caused by larger displacement. In spite of showing good energy dissipation capacity, most of the STE series models have the recentering ratios less than 10%. The STE-0.00 model with zero-friction mechanism even has 13% recentering ratio due to the yielding of the steel bars, thereby producing considerable amount of residual displacement upon unloading. On the contrary, the SMA series models are far superior recentering ratios to the STE series models. The SMA-0.00 model completely goes back to original condition, meaning that this model has 100% recentering ratio. As increasing friction coefficient is applied to the SMA series models, the recentering ratios descend from 100% to 17.7%:

$$\mathrm{RR} = \frac{100\left(\Delta_{\max} - \Delta_{\mathrm{res}}\right)}{\Delta_{\max}}, \tag{3}$$

$$\mathrm{ER} = \frac{100\left(E_{\mathrm{fric}}\right)}{\left(E - E_{\mathrm{fric}}\right)}. \tag{4}$$

The recentering force which is provided by the superelastic SMA bars subjected to reverse phase transformation (F_{SMA,A_f}) directly copes with friction resistance in the bearing system and so plays an important role to restore friction sliders to their original place. The amount of generating residual displacement can be determined by the force ratio of recentering force to friction resistance (FR) force, as defined in (5). The recentering force of the bridge bearing presented herein results in 120 kN (see Figure 9(b)). The SMA-0.10 and SMA-0.15 models were designed with the force ratio almost close to 1.0, indicating that recentering force is nearly equal to friction resistance force. Once the force ratio of the recentering force to friction resistance force falls below 1.0, it tends to decrease recentering capability quickly. In order to

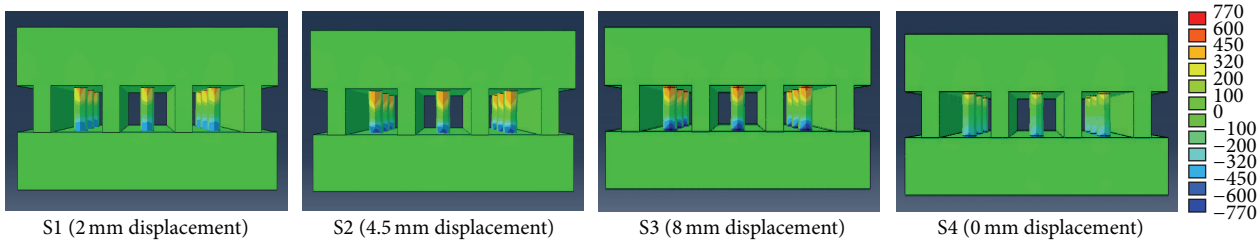

Figure 14: Axial stress component (S22) contours distributed over the STE-0.10 model according to individual loading steps (Unit: Mpa).

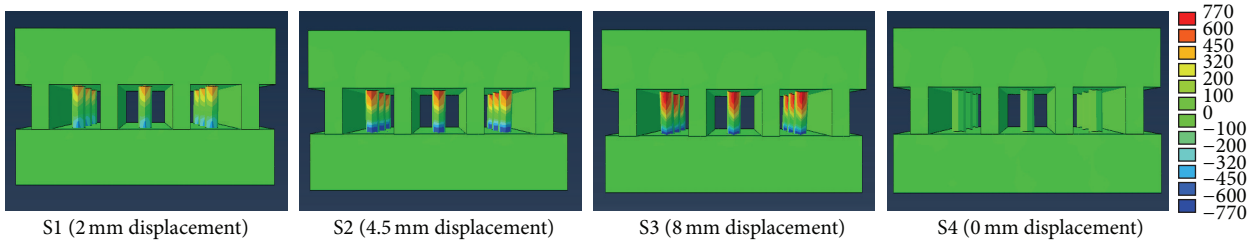

Figure 15: Axial stress component (S22) contours distributed over the SMA-0.10 model according to individual loading steps (Unit: Mpa).

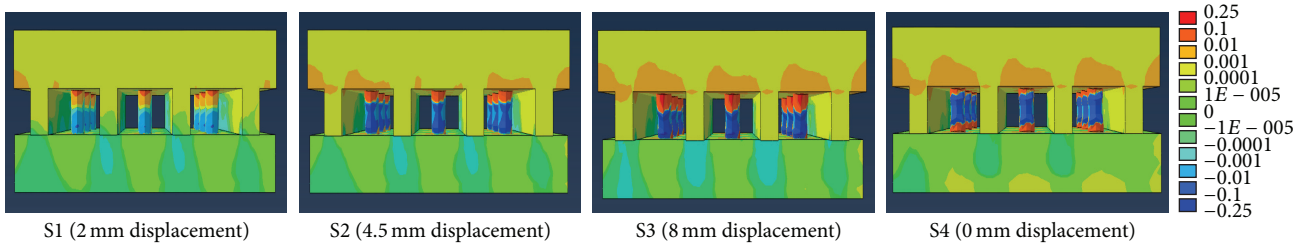

Figure 16: Axial strain component (LE22) contours distributed over the STE-0.10 model according to individual loading steps (Unit: rad).

achieve optimal design with respect to energy dissipation and recentering capability, it is desirable that the bridge bearing model should be designed with recentering force equivalent to friction resistance force:

$$\mathrm{FR} = \frac{F_{\mathrm{SMA},A_f}}{\left|F_{\mathrm{fric,max}}\right|}. \tag{5}$$

6. Observation

The axial stress-strain field contours and curves measured at the specific points (refer to Figure 8) are required to validate the adequacy of FE modeling as well as FE analyses. According to individual loading steps, axial stress component contours distributed over two bridge bearing models with 0.10 friction coefficient are presented in Figures 14 and 15. High stresses concentrate on both fixed ends of the circular bars owing to bending and shear response. The maximum stress field contours are observed after imposing 8 mm displacement. The superelastic SMA bars show higher stress contour levels than the steel bars under the same loading step because they have larger postyield strength at the material properties. In particular, residual stresses even exceeding the yield stress level are observed at the steel bars under the final loading step (S4). This means that additional force is applied to the steel bars for the purpose of returning to their original configuration from residual displacement. On the other hand, nearly zero residual stresses are observed at the superelastic SMA bars when the loading step goes back to zero point. They are restored to original configuration without additional force.

For another investigation, axial strain component contours distributed over two bridge models with 0.1 friction coefficient are displayed at Figures 16 and 17, according to individual loading steps. Similar to the axial stress component contours, high strains concentrate on both fixed ends of the circular bars owing to shear and bending effect while relatively smaller strains are distributed over the middle of the circular bars. The steel bars indicate the considerable amount of residual strain at the final loading step (S4) while the superelastic SMA bars have negligible residual strain upon unloading in the compensation for residual displacement caused by friction mechanism. Both steel plates and friction sliders remain elastic over all loading steps.

The true stress and strain curves obtained from individual measurement points (MP1, PM2, and MP3 points shown in Figure 8) are presented in Figures 18 and 19. The STE-0.10 and SMA-0.10 models are also selected for this investigation. The circular bars are assumed to be the fixed-end beam restrained to rotation and displacement at both end supports.

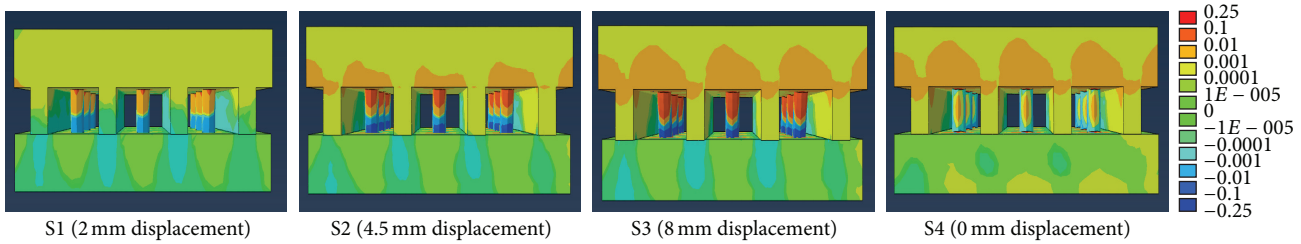

FIGURE 17: Axial strain component (LE22) contours distributed over the SMA-0.10 model according to individual loading steps (Unit: rad).

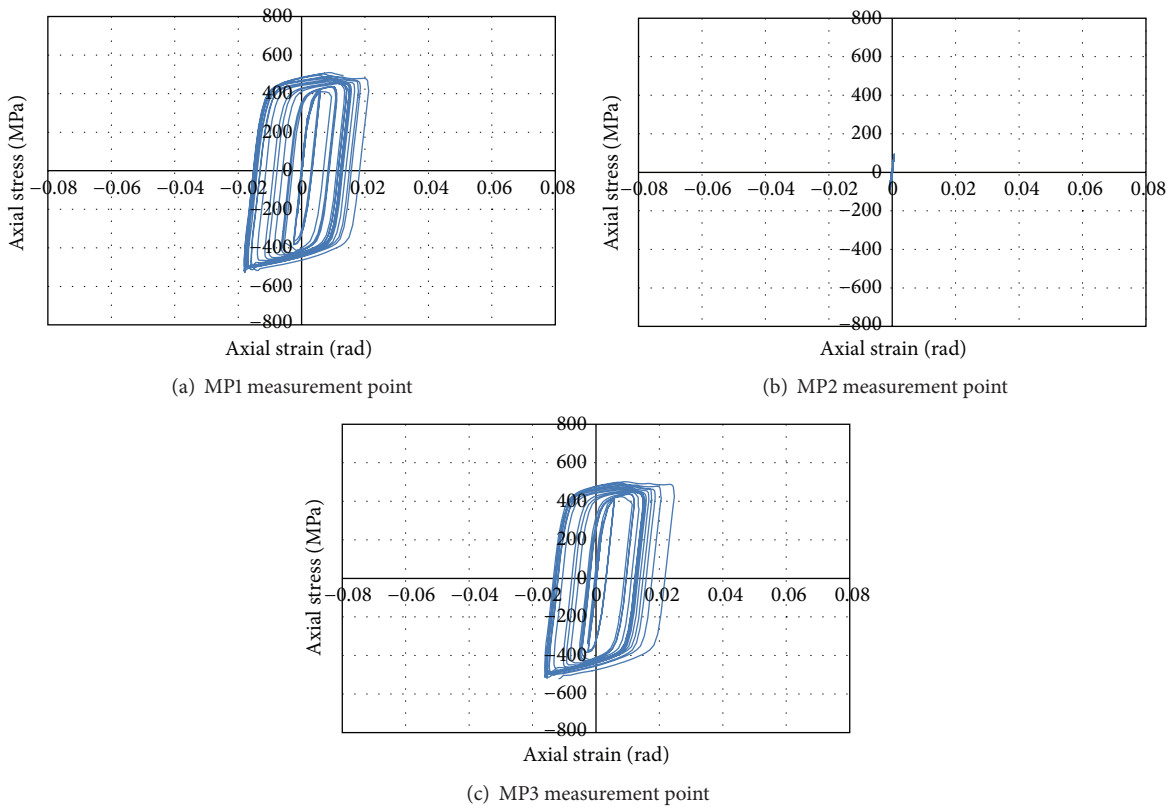

(a) MP1 measurement point

(b) MP2 measurement point

(c) MP3 measurement point

FIGURE 18: True stress and strain curves obtained from individual measurement points (STE-0.10 model).

The concentrated negative bending moment combined with shear force takes place in these end supports. Owing to force concentration, the stress and strain curves measured at the end of the circular bar (MP1 and MP3 point) completely expand into the postyield region and coincide with their base material behavior. For this reason, both isotropic hardening and Bauschinger effect are clearly observed from the measured stress and strain curves of the steel bars. The measured stress and strain curves for the superelastic SMA bars are similar to the flag-shaped hysteresis loops with recentering effect. The middle of the circular bar, which represents the MP2 point, maintains the elastic state. It is thus concluded that the FE models presented herein are able to accurately predict the behavior of the bridge bearing models and to provide reliable results, in lieu of experimental tests.

7. Concluding Remarks

The new bridge bearing systems designed to enhance energy dissipation capacity utilized as friction dampers as well as to add recentering capability introduced by superelastic SMA devices are proposed in this study. The circular bars and the friction sliders are aligned vertically between two plates in the bridge bearing for the purpose of supporting the gravity loads transferred from the superstructure. As for the comparative models, the bridge bearing systems with the conventional steel bars are also designed to validate the superiority of the superelastic SMA bars used for the displacement control device. The FE analyses replaced for the experimental tests are performed to reproduce the cyclic behavior of bridge bearing models under pseudostatic loading with the time history.

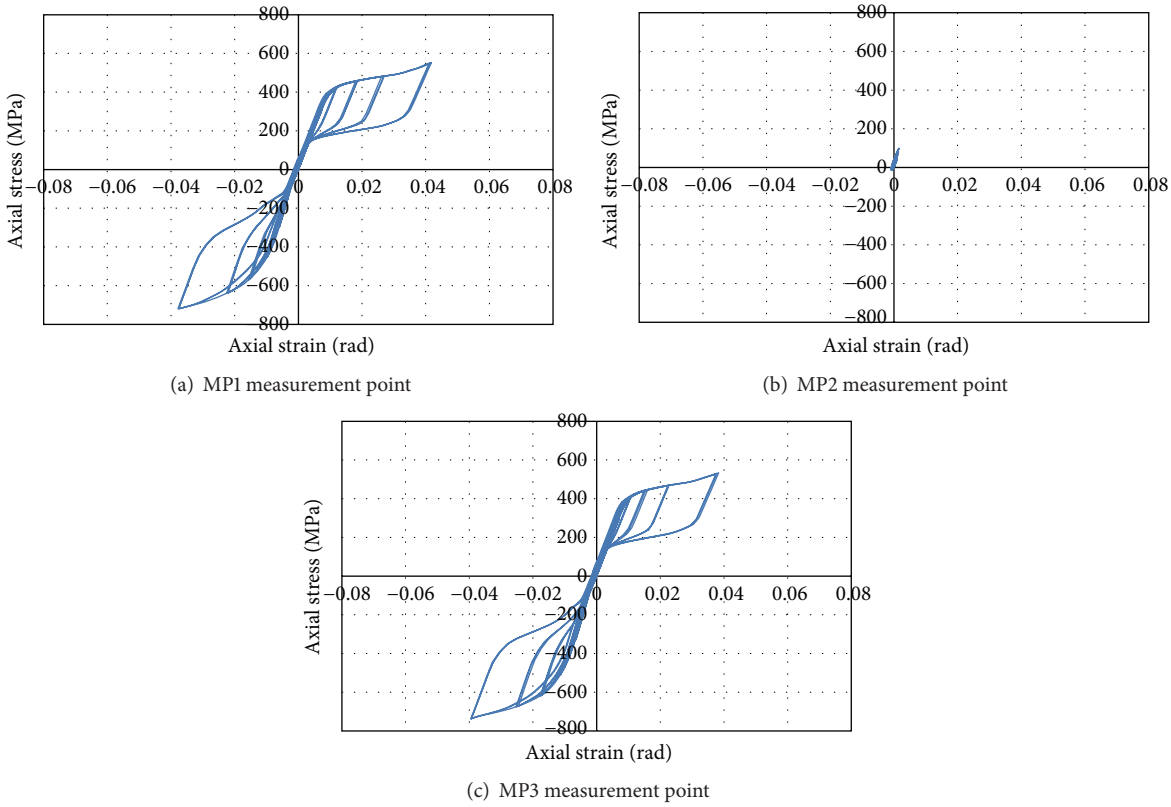

(a) MP1 measurement point

(b) MP2 measurement point

(c) MP3 measurement point

Figure 19: True stress and strain curves obtained from individual measurement points (SMA-0.10 model).

The analysis results confirm the fact that energy dissipation capacity ascends as friction resistance force increases in the bearing system. However, recentering capacity gradually decreases due to increasing residual displacement caused by friction mechanism. The metallic yielding of the steel bars can dissipate higher amount of kinetic energy characterized by the area of the hysteresis loop but cause some drawback of bringing about the considerable amount of residual displacement in the bearing system. In this case, additional force upon unloading should be required to restore original condition without damage. The superelastic SMA bars result in obvious solution to this problem. Once the bridge bearing models equipped with the superelastic SMA bars are designed with recentering force nearly equal to friction resistance force, optimal design for the recentering system will be achieved with respect to recentering capability and energy dissipation capacity at the same time. In spite of recovering from a lot of displacement loading, the superelastic SMA bars in the bridge bearing system show negligible residual stress and strain contours at the original alignment. Finally, the adequacy of FE modeling is guaranteed by the fact that stress and strain curves measured from FE models after analyses are almost similar to their own base material behavior. In the future, the experimental tests intended to establish the practical use of the proposed bearing system will be prepared on the basis of this pilot study result.

Competing Interests

The authors declare that there is no conflict of interests regarding the publication of this paper.

Acknowledgments

This research was supported by a grant (15TBIP-C093001-01) from Support for Infrastructure and Transportation Technology Commercialization Program funded by Ministry of Land, Infrastructure and Transport of Korean government. The authors gratefully acknowledge this support.

References

[1] X. Jiang, X. Qiang, H. Kolstein, and F. Bijlaard, "Analysis on adhesively-bonded joints on FRP-steel composite bridge under combined loading: arcan test and numerical modeling," *Polymers*, vol. 8, no. 1, pp. 1–18, 2016.

[2] A. R. Bhuiyan and M. S. Alam, "Seismic performance assessment of highway bridges equipped with superelastic shape memory alloy-based laminated rubber isolation bearing," *Engineering Structures*, vol. 49, no. 4, pp. 396–407, 2013.

[3] E. T. Filipov, L. A. Fahnestock, J. S. Steelman, J. F. Hajjar, J. M. LaFave, and D. A. Foutch, "Evaluation of quasi-isolated seismic bridge behavior using nonlinear bearing models," *Engineering Structures*, vol. 49, pp. 168–181, 2013.

[4] Z. Pan, C. C. Fu, and Y. Jiang, "Uncertainty analysis of creep and shrinkage effects in long-span continuous rigid frame of Sutong bridge," *Journal of Bridge Engineering*, vol. 16, no. 2, pp. 248–258, 2011.

[5] Y. F. Wang, Y. S. Ma, B. Han, and S. Y. Deng, "Temperature effect on creep behavior of CFST arch bridges," *Journal of Bridge Engineering*, vol. 18, no. 12, pp. 1397–1405, 2013.

[6] O. E. Ozbulut and S. Hurlebaus, "Seismic protection of bridge structures using shape memory alloy-based isolation devices," in *Proceedings of the Structures Congress*, pp. 2066–2077, April 2011.

[7] M. T. A. Chaudhary, M. Abe, Y. Fujino, and J. Yoshida, "System identification of two base-isolated bridges using seismic records," *Journal of Structural Engineering*, vol. 126, no. 10, pp. 1187–1195, 2000.

[8] J. W. Hu, "Response of seismically isolated steel frame buildings with sustainable lead-rubber bearing (LRB) isolator devices subjected to near-fault (NF) ground motions," *Sustainability*, vol. 7, no. 1, pp. 111–137, 2015.

[9] G. P. Warn and A. S. Whittaker, "Vertical earthquake loads on seismic isolation systems in bridges," *Journal of Structural Engineering*, vol. 134, no. 11, pp. 1696–1704, 2008.

[10] J. Seo and J. W. Hu, "Seismic response and performance evaluation of self-centering LRB isolators installed on the CBF building under NF ground motions," *Sustainability*, vol. 8, no. 2, pp. 109–130, 2016.

[11] J. W. Hu and M.-H. Noh, "Seismic response and evaluation of SDOF self-centering friction damping braces subjected to several earthquake ground motions," *Advances in Materials Science and Engineering*, vol. 2015, Article ID 397273, 17 pages, 2015.

[12] J. W. Hu, "Investigation on the cyclic response of superelastic shape memory alloy (SMA) slit damper devices simulated by quasi-static finite element (FE) analyses," *Materials*, vol. 7, no. 2, pp. 1122–1141, 2014.

[13] J. Seo, Y. C. Kim, and J. W. Hu, "Pilot study for investigating the cyclic behavior of slit damper systems with recentering Shape Memory Alloy (SMA) bending bars used for seismic restrainers," *Applied Sciences*, vol. 5, no. 3, pp. 187–208, 2015.

[14] G. Song, N. Ma, and H.-N. Li, "Applications of shape memory alloys in civil structures," *Engineering Structures*, vol. 28, no. 9, pp. 1266–1274, 2006.

[15] R. DesRoches, J. McCormick, and M. Delemont, "Cyclic properties of superelastic shape memory alloy wires and bars," *ASCE Journal of Structural Engineering*, vol. 130, no. 1, pp. 38–46, 2004.

[16] ABAQUS, *ABAQUS 6.12 User's Manuals*, Hibbitt, Karlsson, and Sorensen, Pawtucket, RI, USA, 2013.

[17] F. Auricchio and E. Sacco, "A one-dimensional model for superelastic shape-memory alloys with different elastic properties between austenite and martensite," *International Journal of Non-Linear Mechanics*, vol. 32, no. 6, pp. 1101–1114, 1997.

[18] J. W. Hu, "Numerical simulation for the behavior of superelastic shape memory alloys," *Journal of Mechanical Science and Technology*, vol. 27, no. 2, pp. 381–386, 2013.